Computational Particle Mechanics (2024) 11:657–673
https://doi.org/10.1007/s40571-023-00645-3

Contribution of detonation gas to fracturing reach in rock blasting: insights from the combined finite-discrete element method

Ben Wang[1,2] · **Haibo Li**[1,2]

Received: 5 May 2023 / Revised: 4 July 2023 / Accepted: 4 August 2023 / Published online: 11 September 2023

Abstract
The action of the detonation gas can be considerably affected by the conditions under which the blast occurs. In order to achieve a more comprehensive understanding of the contribution of detonation gas to fracturing reach, the combined finite-discrete element method (FDEM) is performed to modelling rock blasting under three different circumstances: i. single-borehole blasting without free surface under different in situ stress, ii. single- and multi-borehole blasting with a nearby free surface, and iii. underground contour blasting. The results indicated that: (1) detonation gas contributes significantly to the fracturing reach in single-borehole blasting without free surface, but the pneumatic increase factor (*PIF*) decreases with the increase in isotropic in situ stress; (2) under anisotropic in situ stress, the contribution of detonation gas to the fracturing reach is significant in the direction of maximum principal pressure but negligible in the direction of minimum principal pressure; (3) the *PIF* of single-borehole blasting with a nearby free surface is even smaller than that of single-borehole blasting under the hydrostatic pressure of 40MPa, indicating that the nearby free surface weakens the contribution of detonation gas to fracturing reach; (4) due to multi-borehole interaction combined with free surface effect, detonation gas contributes little to the fracturing reach in muti-borehole blasting with a nearby free surface. (5) due to the combined effect of anisotropic in situ stress, free surface and muti-borehole interaction, the contribution of detonation gas to the excavation damage depth can be negligible in underground contour blasting.

Keywords Rock blasting · Detonation gas · Finite-discrete element method · Fracturing reach

1 Introduction

The drill and blast technique is a widely used method to fracture rock in petroleum engineering [1], mining engineering [2], hydropower engineering [3] and nuclear power engineering [4, 5]. Most researchers have accepted that explosive blasting has two consecutive stages which contribute to rock fracturing: (i) the transient action of stress wave and (ii) the quasi-static pressurization driven by the expanding detonation gas [6]. After the explosive is detonated, the detonation products quickly impact the borehole wall and induce radiating shock wave (stress wave) in the surrounding rock. Under the action of the stress wave, a large number of cracks are generated around the borehole, and then, the detonation gas penetrates into the cracks to promote the further propagation of cracks, which is called gas penetration effect. However, how much the detonation gas contributes to rock fracturing is still a question to answer.

A few laboratory and field tests have been conducted to study the effect of detonation gas, but have reached conflicting conclusions. Yang et al. [7] used polymethyl methacrylate (PMMA) as the rock-like material to conduct 2D blasting model experiments with the borehole open and blocked, the results of which showed that the detonation gas greatly increases the fracture zone. Brinkmann [8] conducted blasting experiments with and without borehole liners used to separate the action of detonation gas from the stress wave. His tests results showed that the stress wave controls the damage of back rock, whereas the detonation gas controls the breakout of burden. Olosson et al. [9] used tubular bolts to prevent gas from penetrating the cracks in some boreholes during field bench blasting. It was found that there was no

✉ Haibo Li
hbli@whrsm.ac.cn

1 State Key Laboratory of Geomechanics and Geotechnical Engineering, Institute of Rock and Soil Mechanics, Chinese Academy of Sciences, Wuhan 430071, China

2 University of Chinese Academy of Sciences, Beijing 100049, China

difference in crack lengths between holes charged normally and holes where the charges were inside the bolts, so the detonation gas only separated the already formed blocks. In fact, the action of the detonation gas can be considerably affected by the conditions under which the blast occurs. For example, the contribution of detonation gas to crack generation in deep rock without free surface is different from that of blasting in rock with one or more free surfaces [10].

In addition to experimental tests, numerical modelling is a useful tool for studying problems related to rock blasting due to its time saving and ease of operation. In the finite element method (FEM), the JH2 and RHT material models are usually adopted to simulate rock blasting [11, 12], where the cracks are mimicked by element damage rather than physical discontinuity. Another approach to model cracks in FEM is to delete elements whose stress or deformation exceeds a critical value, but this treatment will lead to unphysical loss of mass and energy [13, 14]. The extended finite element method (XFEM) was also used to analyse gas-driven fractures [15], but it is not capable to capture the generation of random cracks [16]. As a discontinuum-based method, the discrete element method (DEM) is more widely used to simulate rock fracturing and breaking [17–24]. Although the action of detonation gas can be simulated by implementing a pressurization algorithm into the PFC (a commercial software based on DEM) [10], simplifying the mesostructure of rock as bonded discs can lead difficulties to the calculation of gas volume. The discontinuous deformation analysis (DDA) is another discontinuum-based method for studying rock mechanics, which has been used to simulate the action of explosion gas coupled with the rock failure process in bench blasting [25]. However, it is difficult for both pure continuum and discontinuum methods to simulate the whole process of rock failure, which involves the deformation of continuum, the transition from continuum to discontinuum and the movement of discrete bodies [26]. By integrating the advantages of FEM and DEM, Munjiza et al. established the combined finite-discrete element method (FDEM) [27, 28], which is very suitable for modelling rock fracturing and breaking [29–34]. Recently, this hybrid continuum–discontinuum method has been extensively used in rock mechanics and rock engineering to study fracture mechanism of heterogeneous rocks [35], underground excavation [36–39], hydraulic fracturing [40–42], rock blasting [43, 44] and gas-driven fracturing [45].

In the present study, FDEM is performed to modelling rock blasting under three different circumstances: i. single-borehole blasting without free surface under different in situ stress, ii. single- and multi-borehole blasting with a nearby free surface, and iii. underground contour blasting. The contribution of detonation gas to fracturing reach and the corresponding mechanism is analysed. The purpose is to achieve a more comprehensive understanding of the detonation gas effect, so as to provide some guidance for estimating the fracturing reach in rock blasting.

2 FDEM for modelling rock blasting

2.1 Fundamental principles of FDEM

The combined finite-discrete element method (FDEM) was originally developed by Munjiza during the early 1990s. Inspired by the cohesive zone model, he inserted a joint element between every two adjacent solid elements to simulate the initiation and propagation of cracks (as shown in Fig. 1). By incorporating the finite element method (FEM), cohesive zone model and contact mechanics, the FDEM has the capacity to simulate the deformation of continuum, fracturing of solids and the interaction of discrete bodies.

2.1.1 Governing equations

According to Newton's second law, the system governing equation of FDEM can be written as follows

$$\mathbf{M}\ddot{\mathbf{x}} + \mathbf{f}_{\text{int}}(\mathbf{x}) - \mathbf{f}_{\text{ext}}(\mathbf{x}) - \mathbf{f}_{\text{c}}(\mathbf{x}) = 0 \tag{1}$$

where $\mathbf{M}$ is the mass matrix of all nodes; $\mathbf{x}$ is the nodal coordinate vector; $\mathbf{f}_{\text{int}}$, $\mathbf{f}_{\text{ext}}$, and $\mathbf{f}_{\text{c}}$ represent the internal resisting forces, external loads and contact forces, respectively.

The internal forces include the elastic force of solid elements and the bonding force of joint elements [37], which are given by

$$\mathbf{f}_{\text{int}} = \int_{\Omega^{(n)}} \frac{\partial \mathbf{N}}{\partial \mathbf{x}} \mathbf{T} d\Omega + \int_{a^{(n)}} \mathbf{N}\mathbf{t} da \tag{2}$$

where Ω is the domain of interest, $\mathbf{T}$ is the Cauchy stress calculated by the finite element method [46], and $\mathbf{N}$ is the shape function of the solid element [47]. For constant-strain triangular elements used in this paper, $\mathbf{N}_i = \xi\ i$, $i = 1, 2, 3$, $\Sigma \mathbf{N}_i = 1$. $\mathbf{t}$ is the traction caused by the joint elements, and the details can be found in [48].

2.1.2 Contact force

In FDEM, the contact forces are calculated between all contacting discrete bodies and contacting crack surfaces. The normal components are calculated according to the penalty function method [27], which allows the particles to penetrate each other, and the magnitude and distribution of the contact force are directly related to the size and shape of the overlapping area. The penalty function method is an energy-conserving method and has been improved by [48]

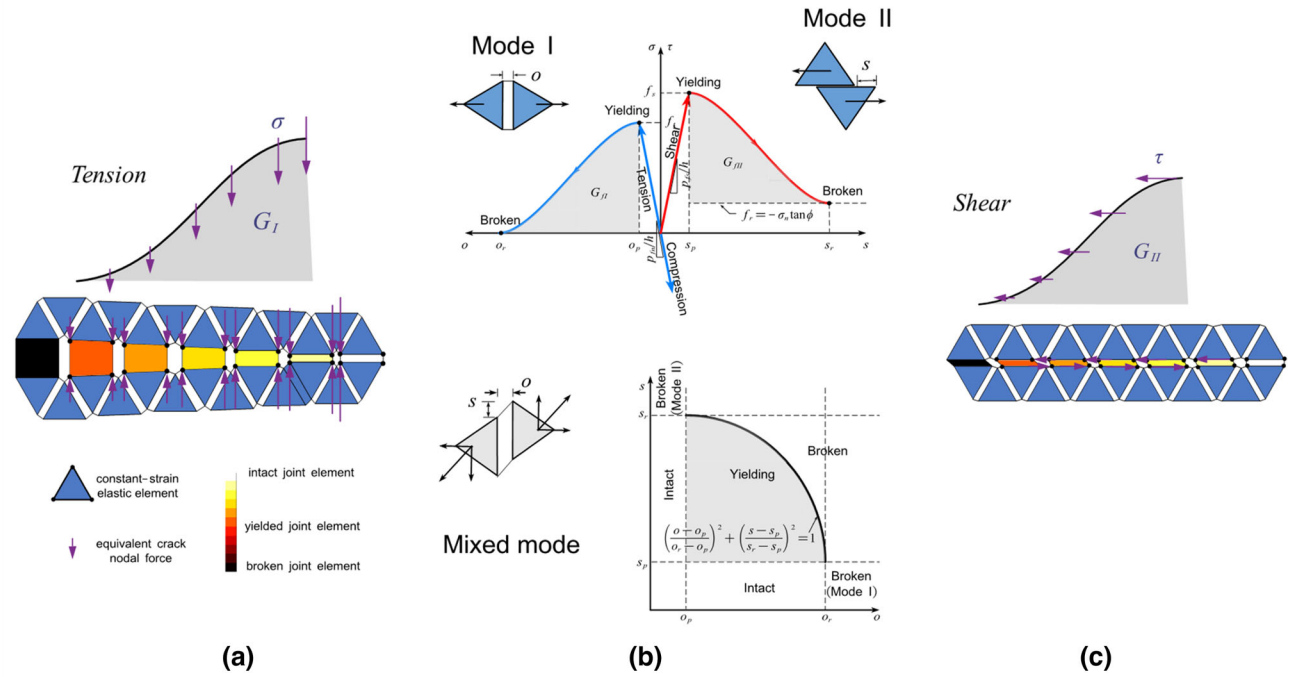

Fig. 1 Fundamental principles of FDEM: **a** Mode I fracture; **b** constitutive behaviour of joint elements; **c** Mode II fracture

to overcome the oscillation problem in the transition from cohesion to contact, whilst the tangential contact force is calculated according to a Coulomb's friction law [49]. Details of the contact force model in the current study can be found in [27, 48, 49].

2.2 The blast loads in the simulation

The explosive load is resolved into the stress wave and detonation gas pressurization. There are various explosive models and equations of state [50] that can be chosen to calculate the explosive load, such as Munjiza's detonation gas model [51] and JWL equation [44]. For the sake of computation convenience, the commonly used Chapman–Jouguet detonation model and power function EOS are adopted in this paper. According to the Chapman–Jouguet theory, the pressure of the detonation product when it begins to expand is

$$p_{\mathrm{e}} = \frac{\rho_{\mathrm{e}} D^2}{2(1+\gamma)} \tag{3}$$

where ρ_{e} is the density of explosive, D is the detonation velocity, and γ is the adiabatic exponent of the detonation product which can be approximately taken as 3 [52].

When the detonation product fills the borehole, its pressure decays to

$$p_{\mathrm{gm}} = \frac{\rho_{\mathrm{e}} D^2}{2(\gamma+1)} \left(\frac{d_{\mathrm{e}}}{d_{\mathrm{b}}}\right)^{2\gamma} \tag{4}$$

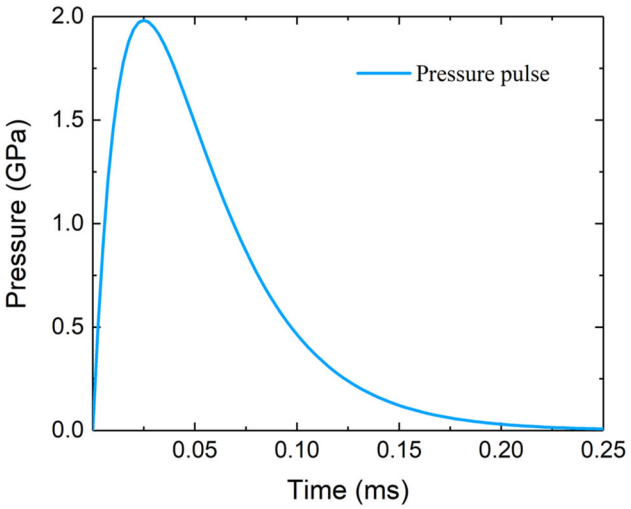

Fig. 2 Pressure pulse acting on the borehole wall

where d_{e} and d_{b} are the diameters of the explosive and the borehole, respectively.

When the detonation product impact the borehole wall, the peak pressure acting on the hole wall is

$$p_m = p_{gm} \cdot n = \frac{\rho_e D^2}{2(1+\gamma)} \left(\frac{d_e}{d_b}\right)^{2\gamma} n \quad (n = 8 \sim 11) \tag{5}$$

In this paper, the magnification factor n is taken as 11.

The pressure pulse acting on the borehole wall is a function of time. The time required for the pressure to reach the peak

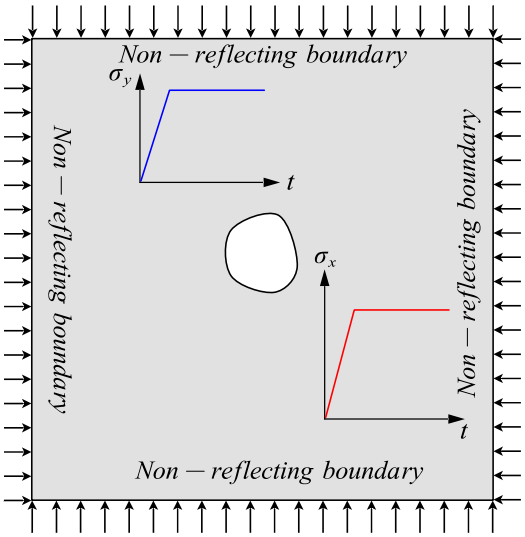

Fig. 3 Dynamic relaxation method in FDEM

Table 1 Input meso-parameters for the numerical model

Parameters	Values
Density, ρ (kg/m^3)	2825
Elastic modulus, E (GPa)	18.0
Poisson's ratio, v	0.17
Damping ratio, k_μ	1.0
Normal penalty of joint elements, p_{fn} (GPa)	540
Tangential penalty of joint elements, p_{fs} (GPa)	540
Tensile strength, f_t (MPa)	6.0
Internal cohesion, c (MPa)	19.0
Internal friction angle, ϕ (°)	40
Mode I fracture energy, G_{fI} (J/m^2)	200
Mode II fracture energy, G_{fII} (J/m^2)	600
Contact penalty, p (GPa)	78.2
Sliding friction angle, ϕ_r (°)	40

value is $t_r = 0.02$–0.03 ms according to the experimental measurements of [53] and [54], whilst the time required for the pressure to decay to 1/10 of the peak pressure is about 4–6 times t_r [55]. Therefore, $t_r = 0.025$ ms is taken, and the function proposed by [56] is adopted to describe the pressure wave acting on the borehole:

$$p_b(t) = 4p_m\left(2^{\frac{-t}{t_r}} - 4^{\frac{-t}{t_r}}\right) \tag{6}$$

In this paper, the density of explosive is $\rho_e = 1.0 \times 10^3$ kg/m^3, the detonation velocity is $D = 3500$ m/s, the charge diameter is $d_e = 0.07$ m, and the borehole diameter is $d_b = 0.1$ m. Substituting these data into Eqs. (3)–(5), $p_{gm} = 180.2$ MPa and $p_m = 1981.7$ MPa can be obtained. According to Eq. (6), the pressure pulse acting on the borehole wall can be obtained as shown in Fig. 2.

Under the dynamic action of the stress wave, many cracks are generated around the borehole, and the penetration of

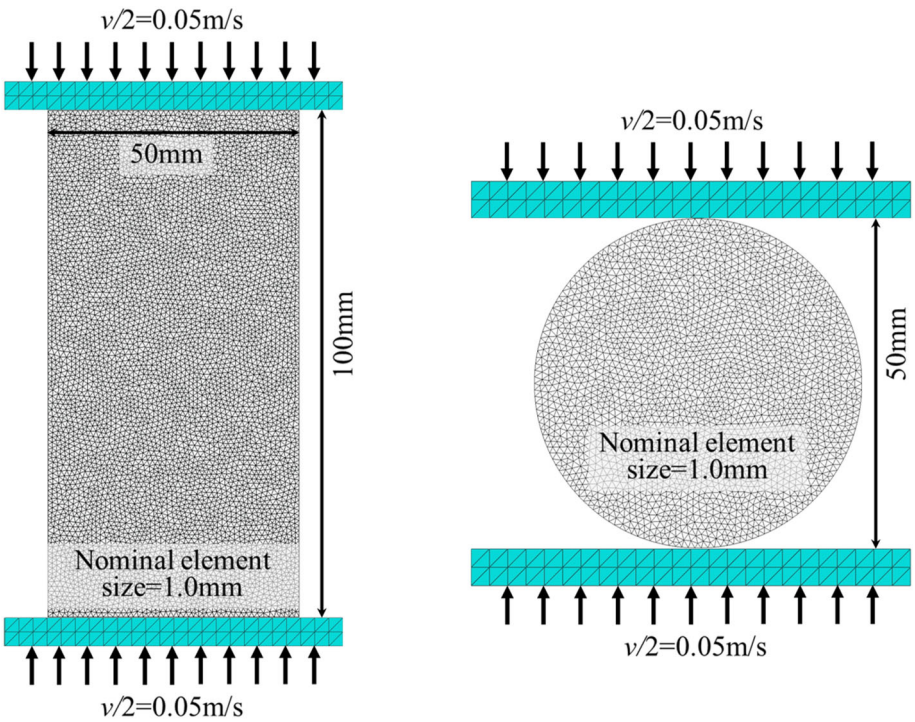

Fig. 4 Numerical model of uniaxial compression and Brazilian splitting tests

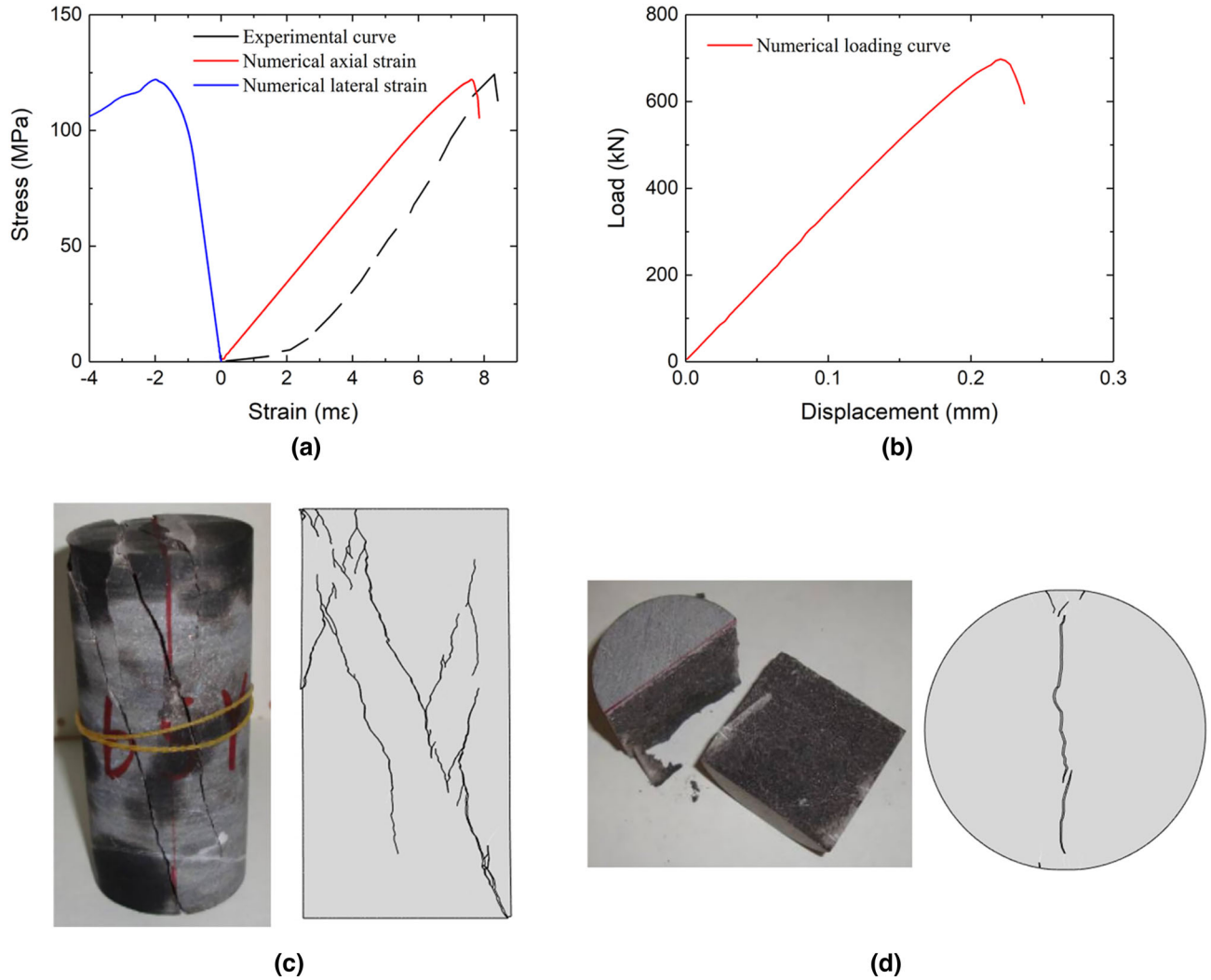

Fig. 5 Numerical simulation results in comparison with experimental results [63]: response curves of **a** uniaxial compression test and **b** Brazilian split test; failure mode of **c** uniaxial compression test and **d** Brazilian split test

Table 2 Macro mechanical properties obtained from experimental tests [63] and numerical simulations

	Elastic modulus, E (GPa)	Poisson's ratio	Uniaxial compressive strength, UCS (MPa)	Brazilian test strength, BTS (MPa)
Experimental	18.0	0.17	123	8.8
Numerical	17.1	0.17	122	8.9

detonation gas can promote these cracks to propagate further. Simultaneously, the pressure of detonation gas decays as the volume expands. This is a complex gas–solid interaction process that is difficult to capture for any numerical method. For the sake of simplification, it is assumed that the gas flow region expands at a constant rate. This treatment was originally proposed by [57] and has been also adopted by other researches about FDEM, and the details of its implementation can be found in [39] and [45].

According to the experimental results of [58], the average flow rate of detonation gas is in the range of 196–279 m/s. In this paper, the expansion rate of gas flow region is taken as 200 m/s, and the gas pressure applied to the borehole wall and connecting cracks is updated at every time step as follows.

$$p_{\mathrm{g}}(t) = p_{\mathrm{gm}}(V_0/V(t))^{\gamma} \tag{7}$$

where V is the current volume of detonation gas[57], and V_0 is the initial volume of borehole.

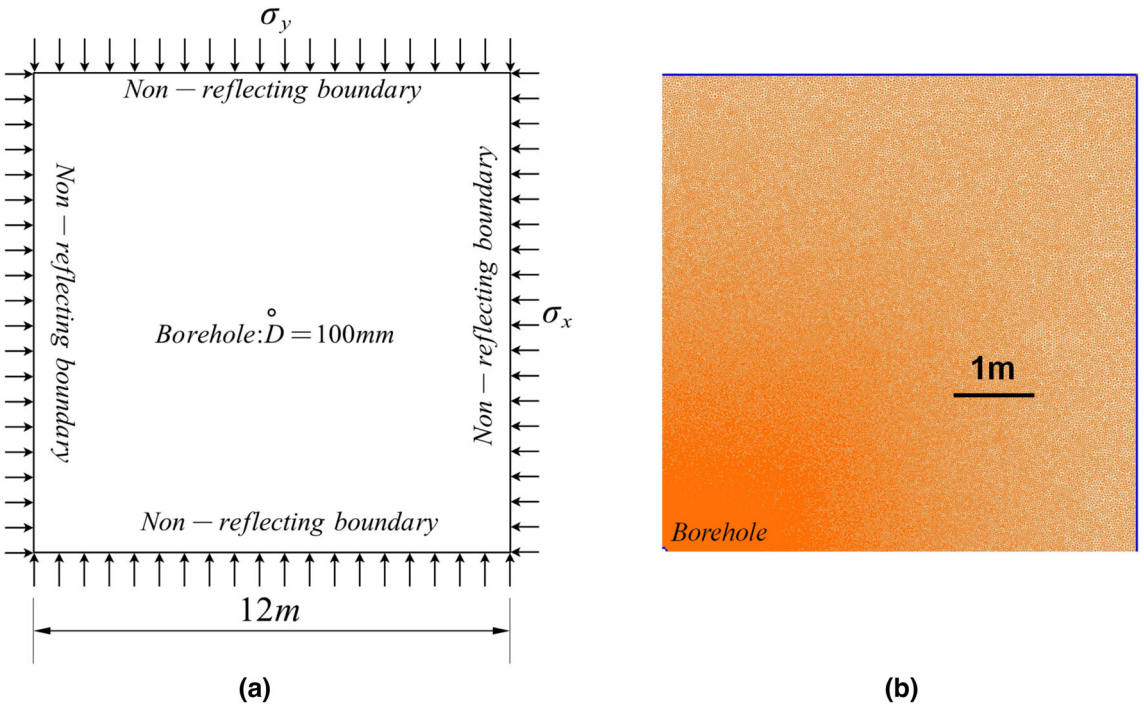

Fig. 6 Simulation of single-borehole blasting without free surface: **a** geometrical model; **b** initial mesh for numerical model

2.3 Non-reflecting boundaries and pre-existing stress

For simulating the propagation of stress wave to infinity, non-reflecting boundaries[59] are usually introduced into the blasting numerical model to reduce the size of the model and save the computational cost. In FDEM, this goal is achieved by applying the following viscous traction on the boundaries:

$$\begin{aligned} t_n &= -\rho c_p \upsilon_n \\ t_s &= -\rho c_s \upsilon_s \end{aligned} \tag{8}$$

where t_n and t_s are the normal and tangential tractions; ρ is the density of rock; v_n and v_s are the normal and tangential velocities; c_p and c_s are the longitudinal and transverse wave velocities.

Before blasting, a static stress field may already exist in the rock, which has a significant effect on the blasting results. In FDEM, the dynamic relaxation method is usually adopted to calculate the pre-existing stress field.

As shown in Fig. 3, the basic principle of the dynamic relaxation method is to apply loads that rise first and then, remain constant on the model boundaries until the maximum nodal velocity in the model is less than a critical value, so as to approach the static equilibrium state. The critical nodal velocity is calculated as follows

$$v_{\mathrm{cr}} = \psi \frac{\min\{\sigma_x, \sigma_y\}}{\rho c_p} \tag{9}$$

where σ_x and σ_y are the two principal in situ stresses, respectively; ψ is a reduction factor, which is taken as 0.001 in this paper.

3 Calibration for the mesoscopic parameters in FDEM

As introduced in Sect. 2.1, many mesoscopic parameters are involved in FDEM, and taking reasonable values of these parameters are the basis of the reliability of the simulation results. For this goal, uniaxial compression and Brazilian splitting numerical tests are usually performed to match the experimental results by trial and error [33, 60].

As shown in Fig. 4, the uniaxial compression numerical model is 50 mm wide and 100 mm high, containing 13,270 triangular elements; and the Brazilian splitting numerical model has a diameter of 50 mm, containing 4512 triangular elements. Both the uniaxial compression and Brazilian splitting simulations use a nominal element size of 1.0 mm and a loading rate of 0.1 m/s. From the previous researches [61, 62], this element size and loading rate are small enough to guarantee the robustness of the simulation results.

The simulated rock is sandstone in this paper, and the input meso-parameters are listed in Table 1. The response curves from numerical simulations and that from experimental tests are shown in Fig. 5a and b, and the basic mechanical properties from simulations and experimental tests are listed

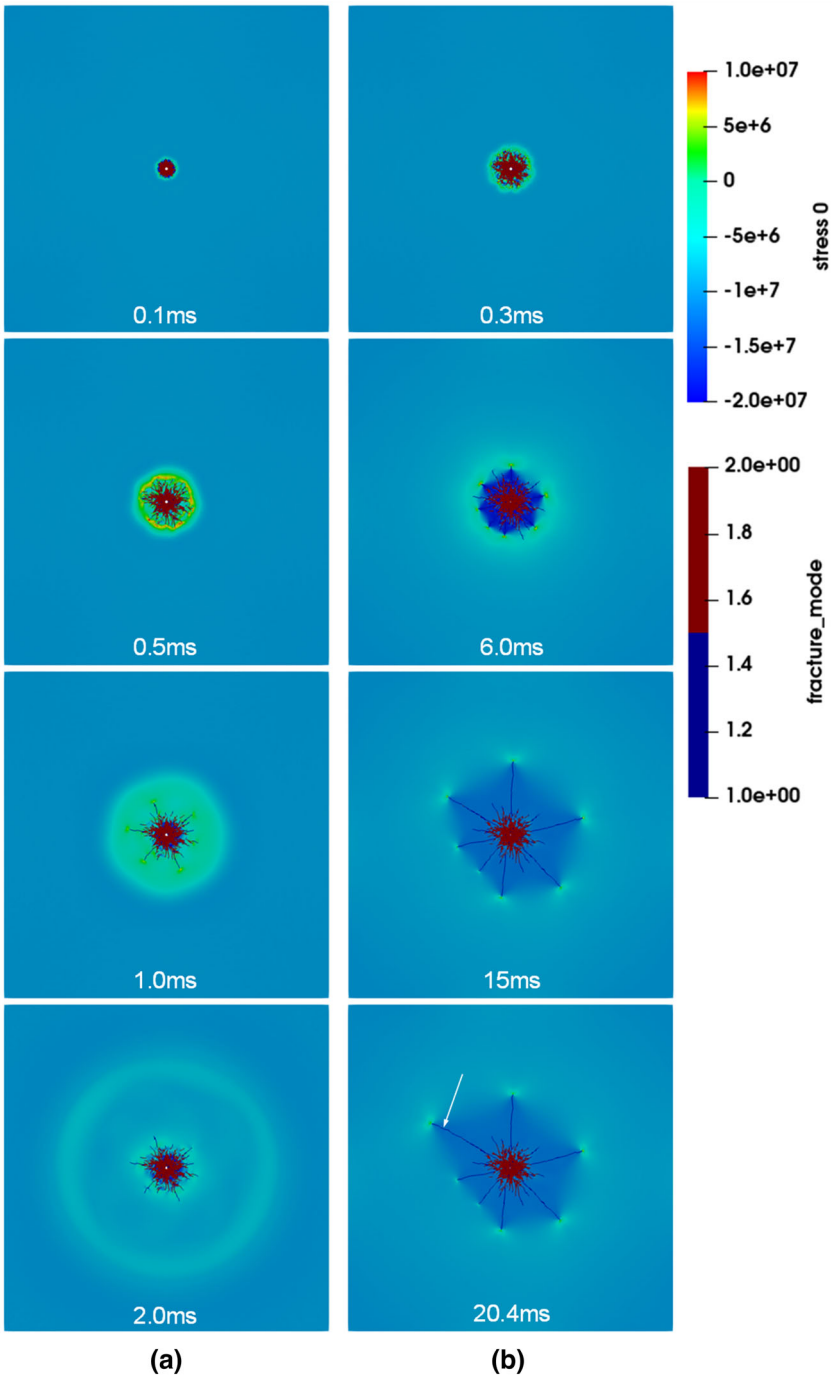

Fig. 7 Stress evolution and fracture process of blasting under the representative in situ stress: **a** without gas pressurization; **b** with gas pressurization

in Table 2, from which it can be seen that the simulation results are very close to experimental results. In addition, the simulated failure patterns are similar to experimental failure patterns (as shown in Fig. 5c and d), which indicated that the input meso-parameters are reasonable.

4 Numerical analysis

In order to investigate the contribution of detonation gas to fracturing reach, this section will use the FDEM introduced in Sect. 2 to simulate rock blasting under three different circumstances: i. single-borehole blasting without free surface, ii. single- and multi-borehole blasting with a nearby free surface, and iii. underground contour blasting. And every

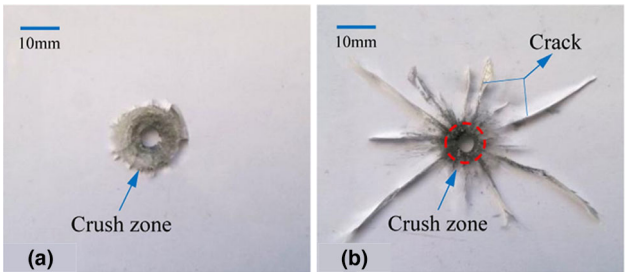

Fig. 8 Crack patterns of experimental blasting [7]: **a** without gas pressurization; **b** with gas pressurization

circumstance includes two scenarios: without gas pressurization and with gas pressurization.

4.1 Single-borehole blasting without free surface

In oil and gas engineering practice, explosive fracturing is sometimes used to enhance the production of wells. The direction perpendicular to the well is approximately infinite, which can be regarded as single-borehole blasting without free surface. As well, single-borehole blasting far away from free surfaces can also be regarded as single-borehole blasting without free surface. Single-borehole blasting without free surface is the simplest circumstance and is the basis for studying other circumstances due to the fact that the effects of free surfaces and the multi-hole interaction are excluded.

As depicted in Fig. 6, a square numerical model with a side length of 12 m centred on a borehole with a diameter of 100 mm was established. The whole model is discretised as an actinomorphic Delaunay mesh containing 490,740 triangular elements, and the maximum and minimum nominal element sizes are 36 mm and 9.8 mm, respectively. The four sides of the model are non-reflecting boundaries to simulate infinite rock mass, and various static initial pressures (σ_x, σ_y) have been applied by dynamic relaxation method before blasting analysis.

4.1.1 Stress evolution and fracture process

Taking the in situ stress ($\sigma_x = \sigma_y = 10$ MPa) as an example, the stress evolution and fracture processes of blasting without gas pressurization are illustrated in Fig. 7a. In the initial stage (before 0.1 ms), the rock near the borehole is crushed under the action of high-intensity compressive stress waves. As the stress wave propagates far away, due to energy consumption and geometric attenuation, its compressive stress is less than the compressive strength of the rock, but the hoop tensile stress can still induce fractures (0.5–1.0 ms). After 1.0 ms, the stress wave is not strong enough to induce fractures and the fracturing reach no longer expands. Connecting the main crack tips will result in a closed convex polygon boundary, and the equivalent fracturing radius is 1.12 m calculated from the area of this convex polygon.

The stress evolution and fracture processes of blasting with gas pressurization are illustrated in Fig. 7b. After the stress wave travels far away (a few ms), the detonation gas has penetrated into the cracks connecting to the borehole. Although the pressure of the detonation gas is much smaller than the stress wave, the gas pressurization on the crack surfaces causes a high degree of stress concentration at the crack tips, so the cracks can propagate to a farther distance. It is worth noting that under the action of gas pressurization, a preferential crack (indicated by the white arrow in Fig. 7) will still propagate whilst the other radial cracks stop propagating, and the mechanism of this phenomenon has been analysed in [64]. During this whole process, the gas pressure decays as the volume increases until all the cracks no longer propagate. The final equivalent fracturing radius is 2.40 m. To evaluate the contribution of detonation gas to the fracturing reach, the ratio of the equivalent fracturing radius under blasting with and without gas pressurization is defined as the pneumatic increase factor (*PIF*):

$$PIF = \frac{2.40m}{1.12m} = 2.14 \tag{10}$$

This indicates that the detonation gas has a significant contribution to the fracturing reach, which is consistent with the previous experimental result [7], as shown in Fig. 8.

4.1.2 Effect of in situ stress

In this section, the effects of isotropic and anisotropic in situ stresses on the pneumatic increase factor (*PIF*) will be studied. The final crack patterns of blasting with and without gas pressurization under different isotropic in situ stresses are shown in Fig. 9, and the variation of equivalent fracturing radius and *PIF* with different isotropic in situ stresses is shown as Fig. 10. It can be seen that, no matter with or without gas pressurization, the equivalent fracturing radius decreases with the increase in isotropic in situ stress, this is because that the isotropic stress is compressive in any direction and thus, inhibits crack propagation. On the other hand, when the isotropic stress is not greater than 40 MPa, the *PIF* is greater than 1.67, indicating that the detonation gas has a significant contribution to the fracturing reach. However, it is interesting to be seen that the *PIF* decreases with the increase in isotropic in situ stress. This is because the peak value of the loading stress wave (~ 1GPa order) is much larger than the gas pressure (10–100 MPa order), so the in situ stress has a greater effect on detonation gas action than that on stress wave action.

In order to investigate the effect of non-isotropic in situ stress, the vertical initial pressure $\sigma_y = 30$ MPa is kept

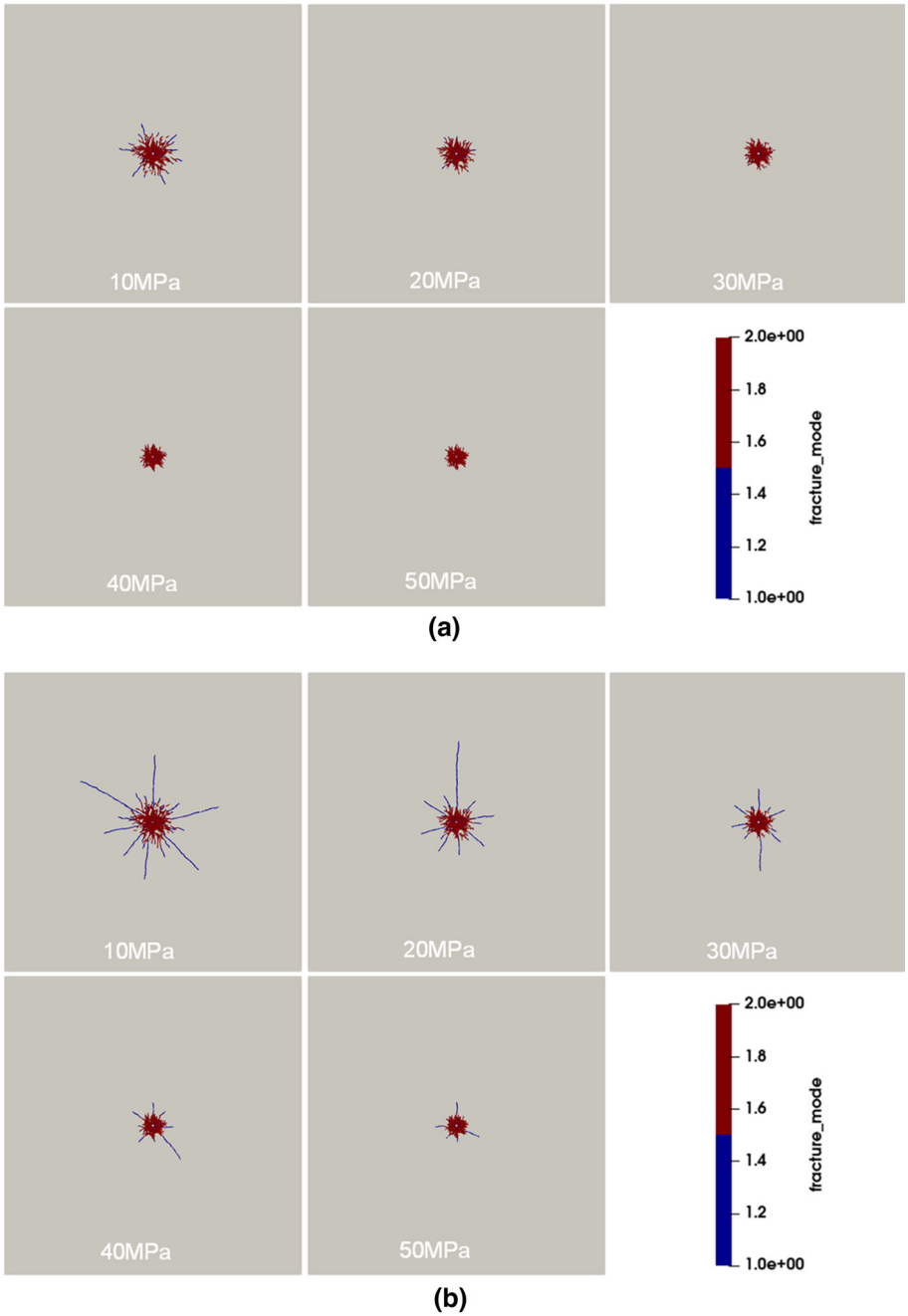

Fig. 9 Final crack patterns of blasting under different isotropic in situ stresses: **a** without gas pressurization; **b** with gas pressurization

constant, and the lateral pressure coefficient ($\lambda = \sigma_x/\sigma_y$) is changed from 1/3 to 1. The final crack patterns of blasting with and without gas pressurization under non-isotropic in situ stresses are shown in Fig. 11, and the variation of equivalent fracturing reach and *PIF* with different lateral pressure coefficients is shown as Fig. 12. It can be seen that non-isotropic in situ stresses lead to non-uniform crack patterns, that is, fracturing reach in the direction of major initial pressure (σ_y) is farther than that in the minor initial pressure (σ_x). This is due to the fact that the initial hoop compressive stress in the direction of σ_x is greater than the initial hoop compressive stress in the direction of σ_y, thereby inhibiting the crack propagation in the direction of σ_x. Moreover, under any non-isotropic in situ stresses, the *PIF* in the direction of σ_y is larger than that in the direction of σ_x, indicating that the detonation gas increases the non-uniformity of crack propagation. This is due to the competitive advantage of long cracks in propagating compared to short cracks under the action of gas pressurization[64]. It is worth noting that when the lateral pressure coefficient decreases (the difference between σ_x and σ_y increases), the *PIF* in the direction of minor principal pressure (σ_x) decreases and tends to 1,

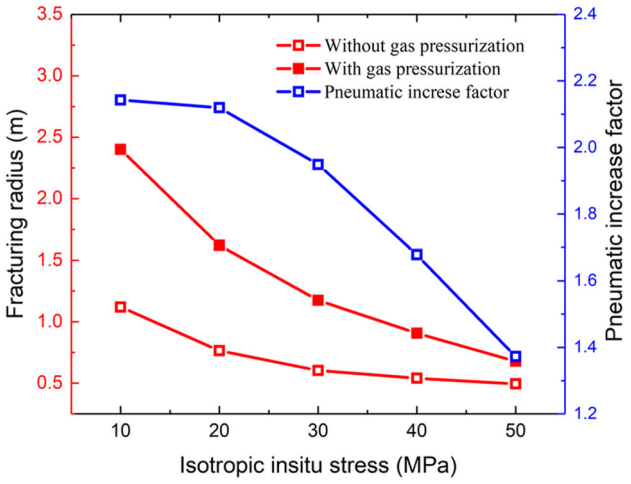

Fig. 10 Variation of equivalent fracturing radius and *PIF* with different isotropic in situ stresses

indicating that the contribution of detonation gas on fracturing reach in the direction of minor principal in situ stress can be ignored.

4.2 Blasting with a nearby free surface

In engineering practice (such as bench blasting), there is usually a nearby free surface parallel or sub-parallel to the boreholes. Under this circumstance, both the nearby free surface and multi-hole interaction could influence the action of the detonation gas. This section will first investigate the contribution of detonation gas on fracturing reach in single-borehole blasting with a nearby free surface and then, investigate the contribution of detonation gas on fracturing reach in multi-borehole blasting with a nearby free surface.

4.2.1 Single-borehole blasting with a nearby free surface

A 24 m × 14 m single-borehole blasting model containing 17,522 triangular elements is established as shown in Fig. 13a and b, the minimum and maximum element size are 9.8 mm and 93 mm, respectively. The upper side is the free surface, and the other three sides are non-reflecting boundaries. The borehole is located 2 m away from the free surface on the central axis. The final crack patterns of single-borehole blasting with and without gas pressurization are shown in Fig. 14a and b. It can be seen that the damage depth (the furthest distance of crack propagation in the direction vertical to the free surface) is 2.26 m in the blasting without gas pressurization, whilst the damage depth is 3.76 m in the blasting with gas pressurization. The pneumatic increase factor (*PIF*) is calculated as 3.76/2.26 = 1.66, which is even smaller than that in blasting under the in situ stress of ($\sigma_x = \sigma_y = 40$ MPa), indicating that the existence of the free surface weakens the effect of the gas. On the one hand, this is because the tensile stress wave reflected from the free surface makes the burden rock more broken and provides more channels for gas flow, and on the other hand, the burden rock is easier to move to the outside of the free surface, making the gas easier to expand.

4.2.2 Multi-borehole blasting with a nearby free surface

The 5-borehole blasting model containing 314,747 triangular elements is shown in Fig. 13c and d, the borehole spacing is 1.5 m, and the other dimensions and boundary conditions are the same as that of the single-hole blasting model. The final crack patterns of 5-borehole blasting with and without gas pressurization are shown in Fig. 14c and d. Intuitively, the difference in the fracturing reach between blasting with and without gas pressurization is not very significant. The damage depths of the end hole in blasting with and without gas pressurization are 6.21 m and 4.53 m, respectively, so the *PIF* is 1.37, whilst the damage depth of the central hole in blasting with and without gas pressurization is 1.39 m and 1.44 m, respectively, so the *PIF* is 0.97. This indicates that the damage of the back rock in bench blasting is dominated by stress wave, which is consistent with the conclusion from field tests of Brinkmann [8]. The explanation of this phenomenon is that the cracks connecting boreholes makes it easier for the rock to move perpendicular to the borehole line, which makes the gas pressure attenuate faster combined with the free surface effect explained in Sect. 4.2.1.

4.3 Underground contour blasting

Contour blasting is an excavation method often used in tunnelling, and the effects of in situ stress, free surfaces and multi-borehole interaction are all involved under this circumstance. In order to investigate the effect of detonation gas on excavation damage in contour blasting, a numerical model is established as shown in Fig. 15. The side length of the model is 24 m, the diameter of the design contour surface is 4 m, the burden is 0.9 m, and 16 boreholes with a diameter of 0.1 m are uniformly arranged on the design contour surface. The horizontal in situ stress of 30 MPa and the vertical in situ stress of 20 MPa have been applied before blasting, and the in situ stress computation result is shown in Fig. 16.

The simulated final crack patterns of contour blasting with and without gas pressurization are shown in Fig. 17a and b. Intuitively, the difference in damage depth of any direction between the two scenarios is not obvious. In order to further reveal the contribution of detonation gas on the damage depth (fracturing reach) of contour blasting, the damage depth in various directions is depicted as shown in Fig. 18. It can be seen that no matter in which direction, the damage depths of contour blasting with and without gas pressurization are very close, indicating that detonation gas contributes little to

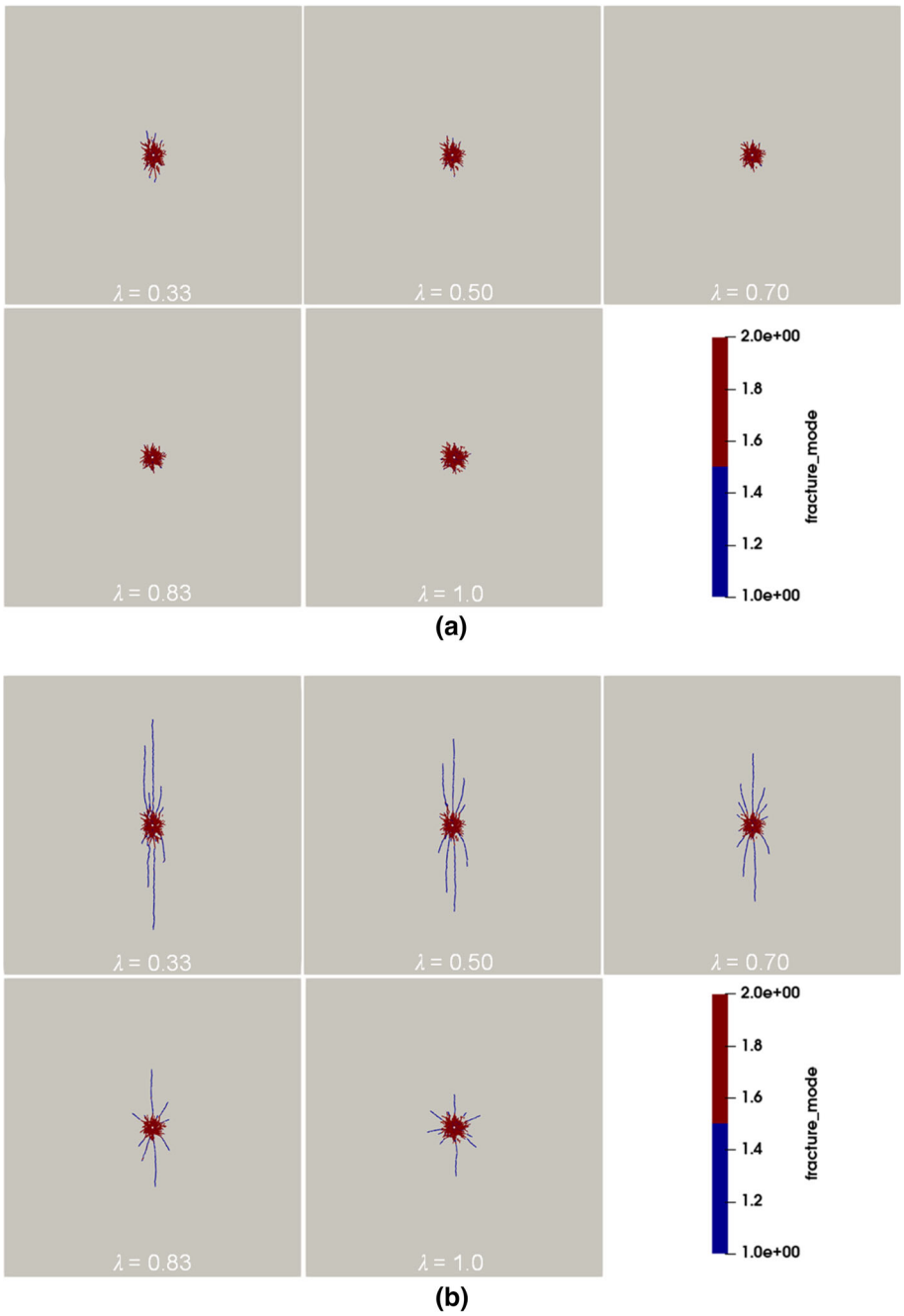

Fig. 11 Final crack patterns of blasting under non-isotropic in situ stresses: **a** without gas pressurization; **b** with gas pressurization

the damage depth in contour blasting. This phenomenon is the result of the three effects of in situ stress, free surface and multi-borehole interaction. First, from the perspective of in situ stress effect, the maximum principal pressure of the borehole is sub-parallel to the design contour surface (see Fig. 16c), so that the detonation gas makes little contribution to the crack propagation in the direction perpendicular to the design contour surface (as explained in Sect. 4.1.2). Secondly, from the perspective of the free surface effect, the existence of the free surface weakens the action of detonation gas (as explained in Sect. 4.2.1). Third, the multi-borehole effect further reduces the contribution of detonation gas to the damage depth (as explained in Sect. 4.2.2).

5 Discussion

As mentioned before, the effect of detonation gas in rock blasting is a complex and vague problem that is difficult to carry out experimental research. Although some experimental tests have been carried out, the conclusions reached are not all consistent. [7] concluded that detonation gas can

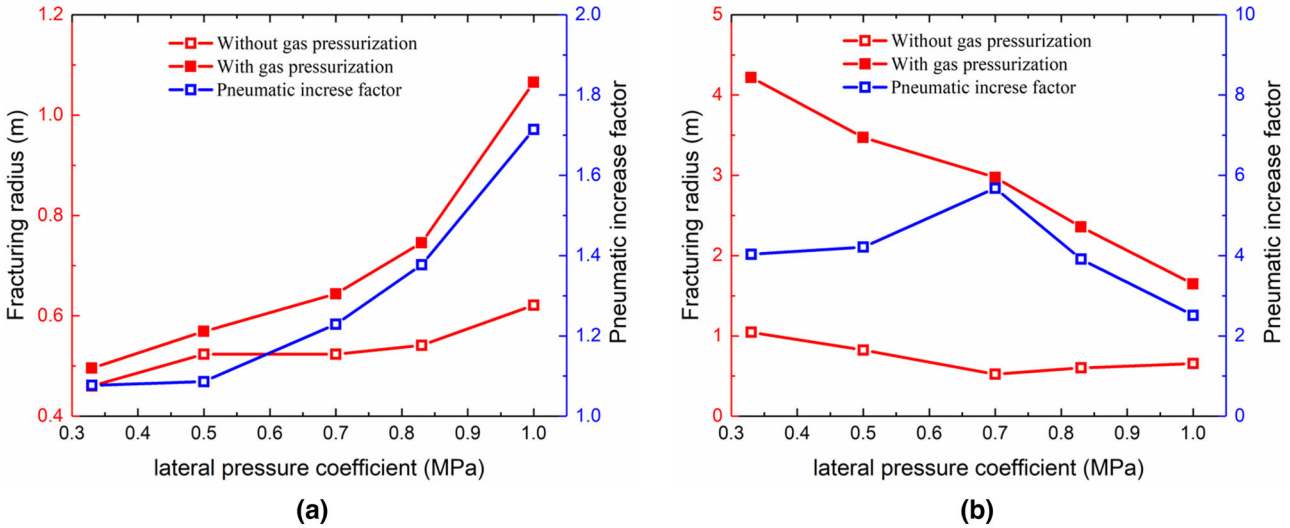

Fig. 12 Variation of equivalent fracturing reach and *PIF* with different lateral pressure coefficients: **a** in the direction of minimum principal pressure; **b** in the direction of maximum principal pressure

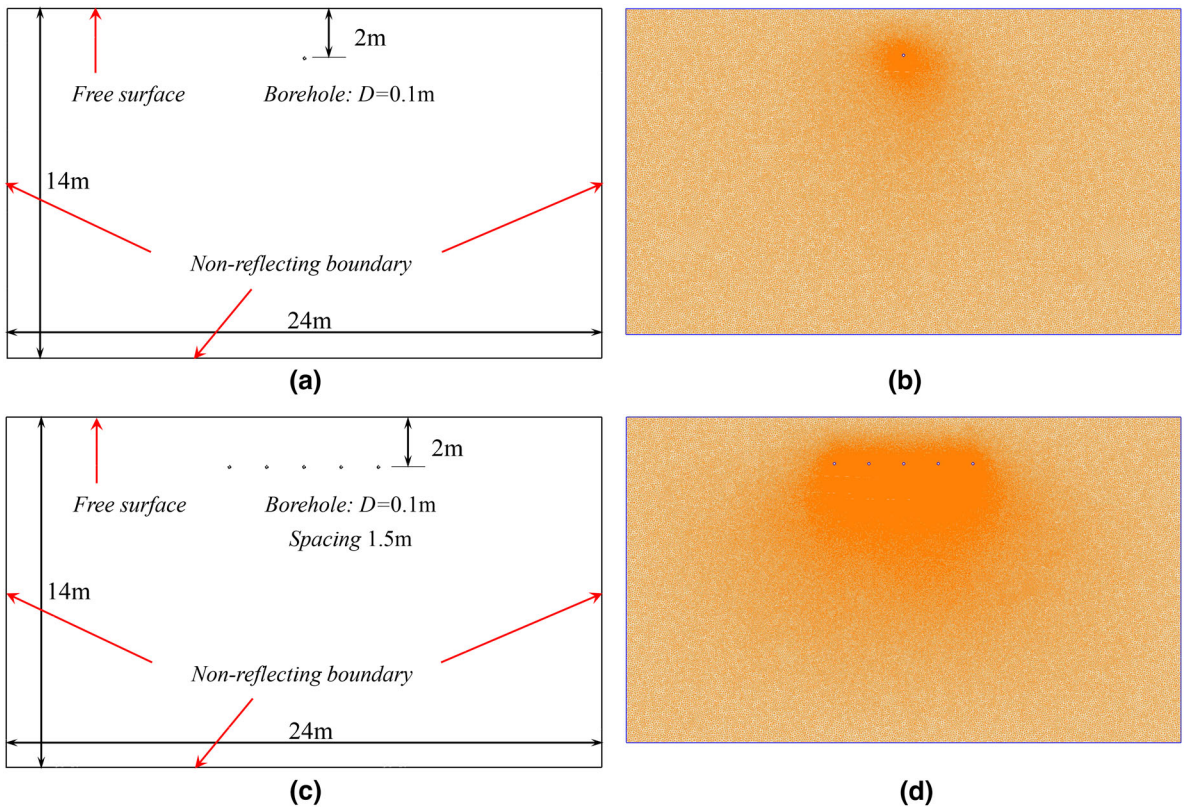

Fig. 13 Simulation of blasting with a nearby free surface: **a** geometrical model of single-borehole blasting; **b** numerical model of single-borehole blasting; **c** geometrical model of multi-borehole blasting; **d** numerical model of multi-borehole blasting

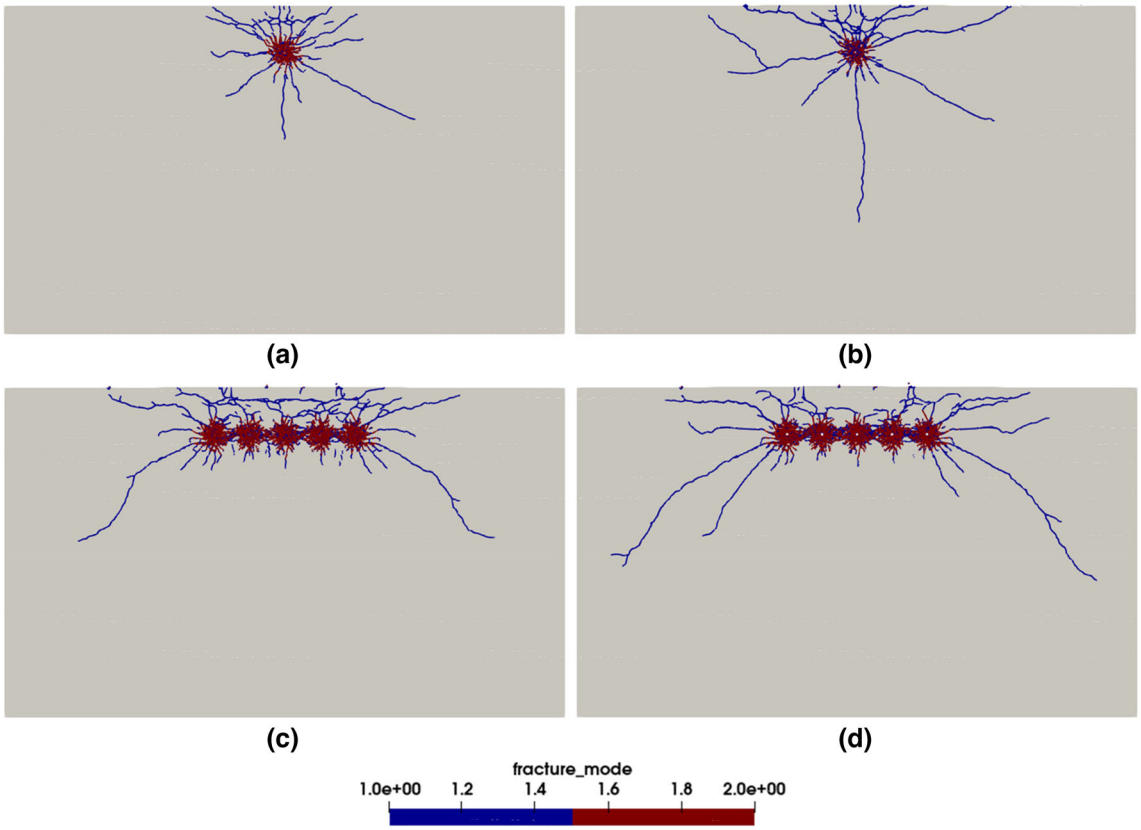

Fig. 14 Final crack patterns blasting with a nearby free surface: **a** single-borehole blasting without gas pressurization; **b** single-borehole blasting with gas pressurization; **c** multi-borehole blasting without gas pressurization; **d** multi-borehole blasting wit gas pressurization

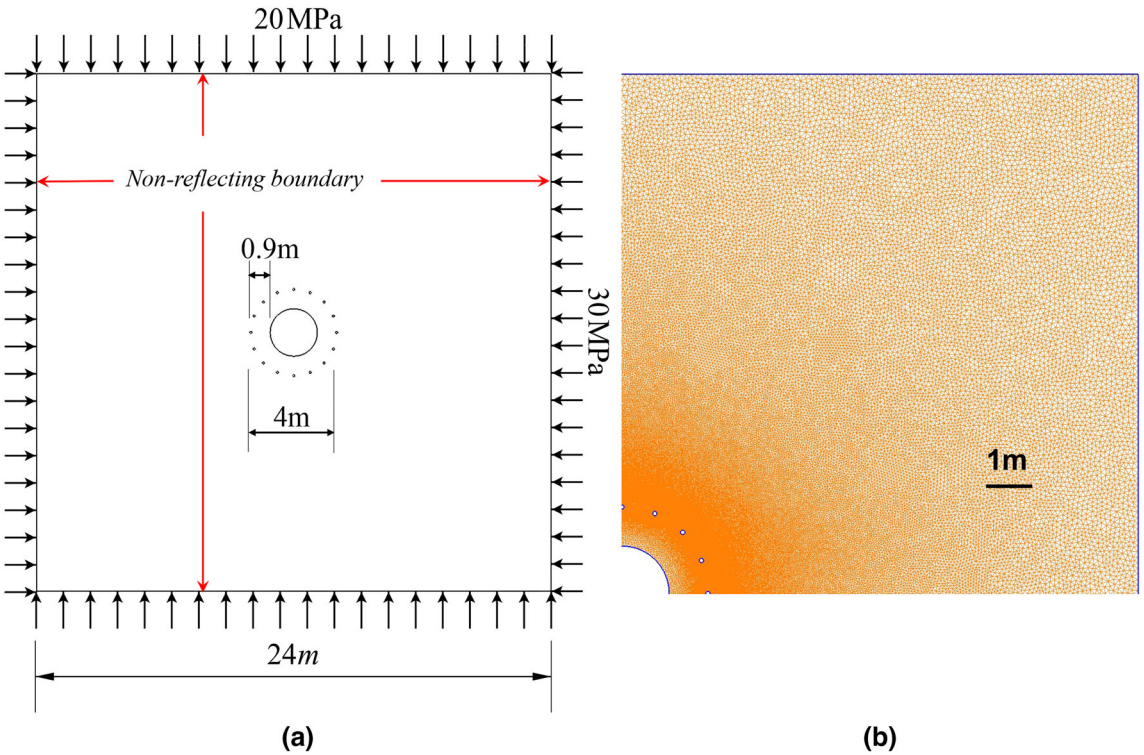

Fig. 15 Simulation of underground contour blasting: **a** geometrical model; **b** numerical model

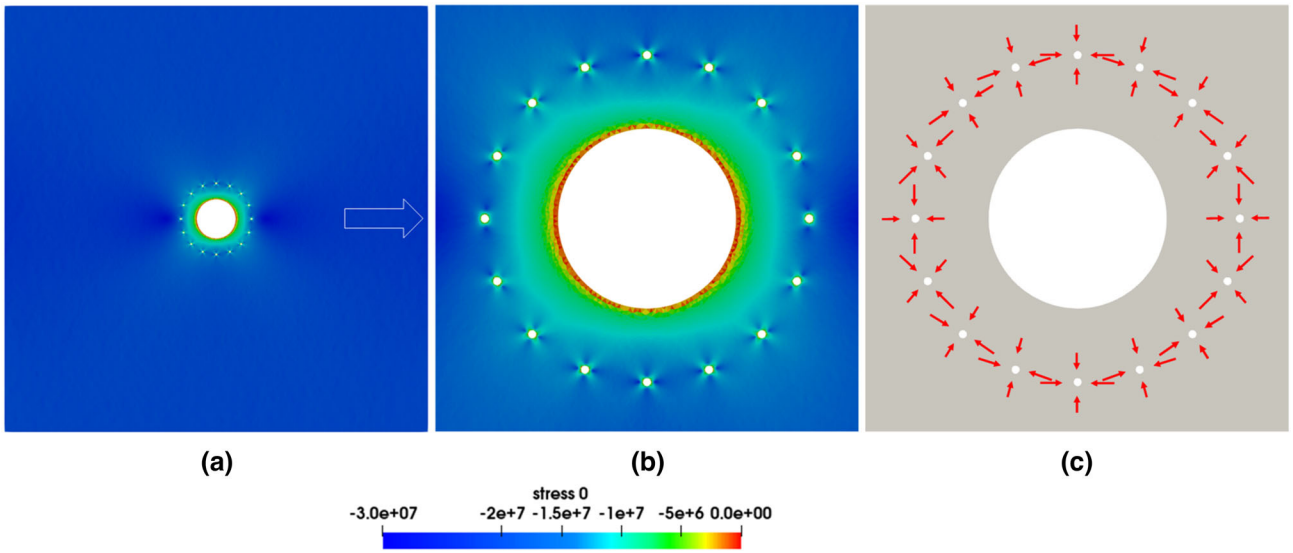

Fig. 16 Distribution of initial static stress: **a** maximum principal stress; **b** partial enlargement; **c** local compression state of boreholes

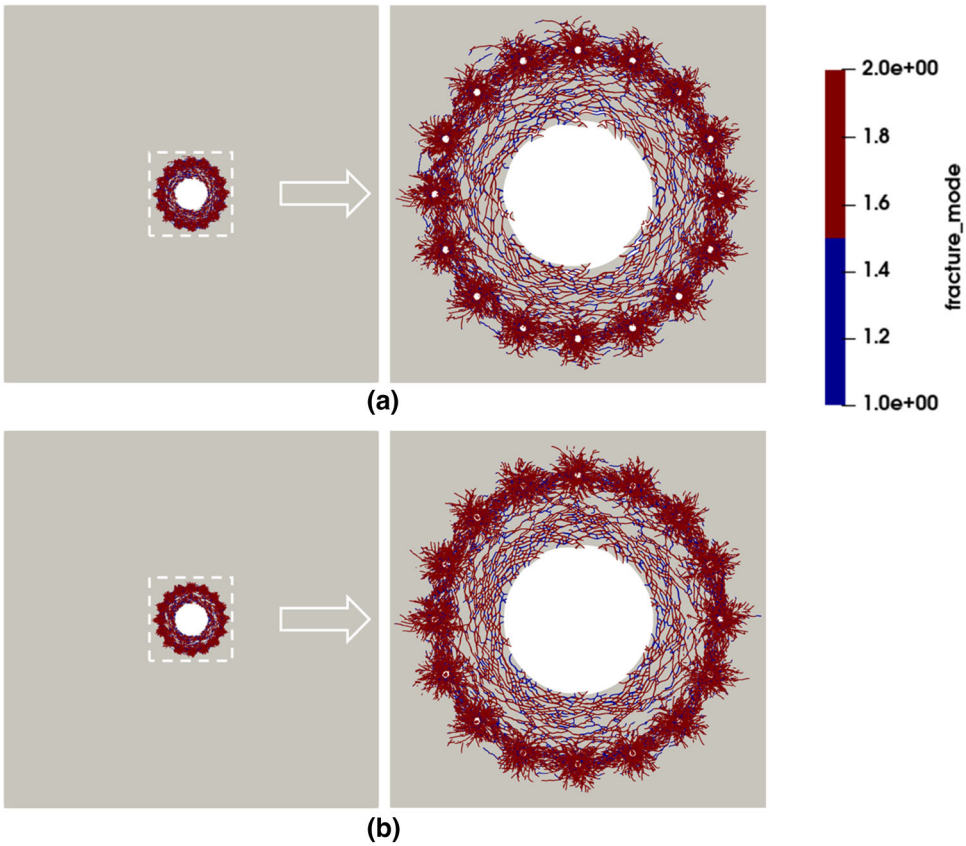

Fig. 17 Final crack patterns of contour blasting: **a** without gas pressurization; **b** with gas pressurization

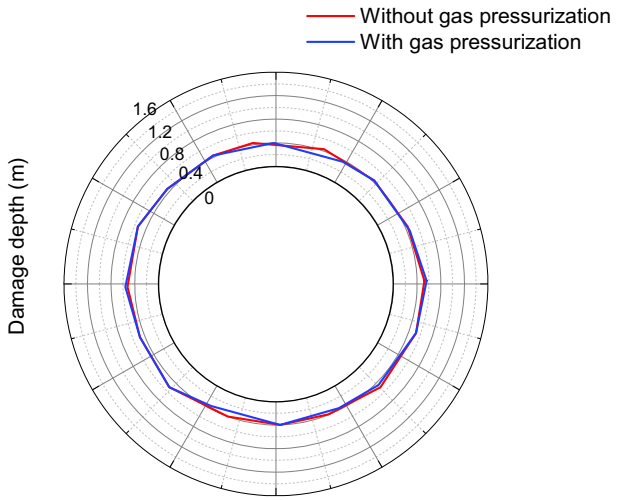

Fig. 18 Damage depth in various directions

increase the crack lengths by more than three times, but [9] indicated that the detonation gas has little influence on the crack lengths. The experimental results of [8] showed that the detonation gas controls the breakout of burden but has little influence on the fracturing of back rock. The role of detonation gas is actually greatly influenced by the conditions under which the blast occurs. For example, [65] indicated that the burden has a significant effect on the role of stress wave and gas pressure in both single-hole and multi-hole tests, and the experimental results of [66] indicated that the increase in confining pressure reduces the contribution of gas pressure to crack length.

As a hybrid continuum–discontinuum numerical method, the combined finite-discrete element method (FDEM) is a useful tool to simulate fluid flow through cracks[41, 67, 68]. In order to study the contribution of detonation gas to the fracturing reach, the combined finite-discrete element method (FDEM) is used to perform numerical simulations of rock blasting under different circumstances in this paper. Part of the simulation results are in consistent with that of experiments or field tests, which verifies the reliability of this study to a certain extent.

However, due to the inherent limitations of the numerical method used in this paper, the effect of the detonation gas may be overestimated. On the one hand, ignoring the initial compaction stage of rock deformation (see Fig. 5a) will lead to an underestimation of rock deformation, thereby underestimating the attenuation of gas pressure with volume increase. On the other hand, in practical blasting, part of the detonation gas will escape from the borehole collar or the cracks to the atmosphere, which weakens the action of the detonation gas. Nevertheless, the present findings are still significant to serve as a reference to insight the contribution of detonation gas to the fracturing reach in rock blasting and provide some guidance for practical blasting such as estimating the fracturing or damage range.

6 Conclusions

In order to investigate the contribution of detonation gas to fracturing reach under different occurrence conditions, the combined finite-discrete element method (FDEM) is used to simulate rock blasting of three different circumstances: i. single-borehole blasting without free surface under different in situ stress, ii. single- and multi-borehole blasting with a nearby free surface, and iii. underground contour blasting. According to the numerical modelling, the following conclusions can be drawn:

(1) In single-borehole blasting without free surface, detonation gas contributes significantly to the fracturing reach, which is consistent with previous experimental results. However, the pneumatic increase factor (*PIF*) decreases from 2.14 to 1.37 when the isotropic in situ stress (hydrostatic pressure) increases from 10 to 50 MPa.
(2) Under anisotropic in situ stress, the contribution of detonation gas to the fracturing reach is significant in the direction of maximum principal pressure but negligible in the direction of minimum principal pressure.
(3) The *PIF* of single-borehole blasting with a nearby free surface is 1.66, which is even smaller than that of single-borehole blasting under the hydrostatic pressure of 40 MPa, indicating that the nearby free surface weakens the contribution of detonation gas to fracturing reach.
(4) Due to multi-borehole interaction combined with free surface effect, detonation gas contributes little to the fracturing reach in muti-borehole blasting with a nearby free surface (bench blasting), which is consistent with the conclusion from field tests.
(5) Due to the combined effect of anisotropic in situ stress, free surface and muti-borehole interaction, detonation gas contributes little to the excavation damage depth in underground contour blasting.

Acknowledgements This work is supported by the National Key R&D Program of China (2020YFA0711802), National Nature Science Foundation of China (U22A20239) and Wuhan Science and Technology Bureau of China. We would like to thank Dr. Xiaofeng Li for his suggestions on manuscript writing. The authors acknowledge the constructive comments from the anonymous reviewers and the editor.

Declarations

Conflict of interest The authors declare that they have no known competing financial interests or personal relationships that could have appeared to influence the work reported in this paper.

References

1. Lak M, Fatehi Marji M, Yarahmadi Bafghi A, Abdollahipour A (2019) A coupled finite difference-boundary element method for modeling the propagation of explosion-induced radial cracks around a wellbore. J Nat Gas Sci Eng. https://doi.org/10.1016/j.jngse.2019.01.019
2. Konicek P, Soucek K, Stas L, Singh R (2013) Long-hole destress blasting for rockburst control during deep underground coal mining. Int J Rock Mech Min Sci. https://doi.org/10.1016/j.ijrmms.2013.02.001
3. Hu YG, Liu MS, Wu XX, Zhao G, Li P (2018) Damage-vibration couple control of rock mass blasting for high rock slopes. Int J Rock Mech Mining Sci 103:137–144. https://doi.org/10.1016/j.ijrmms.2018.01.028
4. Haibo L, Xiang X, Jianchun L et al (2011) Rock damage control in bedrock blasting excavation for a nuclear power plant. Int J Rock Mech Min Sci. https://doi.org/10.1016/j.ijrmms.2010.11.016
5. Li XF, Li HB, Zhang GK (2019) Damage assessment and blast vibrations controlling considering rock properties of underwater blasting. Int J Rock Mech Min Sci 121:10405. https://doi.org/10.1016/j.ijrmms.2019.06.004
6. Kutter HK, Fairhurst C (1971) On the fracture process in blasting. Int J Rock Mech Min Sci. https://doi.org/10.1016/0148-9062(71)90018-0
7. Yang R, Ding C, Yang L et al (2018) Visualizing the blast-induced stress wave and blasting gas action effects using digital image correlation. Int J Rock Mech Min Sci. https://doi.org/10.1016/j.ijrmms.2018.10.007
8. Brinkmann JR (1990) An experimental study of the effects of shock and gas penetration in blasting. In: Proceedings of the 3rd international symposium on rock fragmentation by blasting. Brisbane Australia, pp 55–66
9. Olsson M, Nie S, Bergqvist I, Ouchterlony F (2002) What causes cracks in rock blasting? Fragblast 6:221–233
10. Yuan W, Su X, Wang W et al (2019) Numerical study of the contributions of shock wave and detonation gas to crack generation in deep rock without free surfaces. J Pet Sci Eng. https://doi.org/10.1016/j.petrol.2019.02.004
11. Ma GW, An XM (2008) Numerical simulation of blasting-induced rock fractures. Int J Rock Mech Min Sci 45:966–975. https://doi.org/10.1016/j.ijrmms.2007.12.002
12. Jayasinghe LB, Shang J, Zhao Z, Goh ATC (2019) Numerical investigation into the blasting-induced damage characteristics of rocks considering the role of in-situ stresses and discontinuity persistence. Comput Geotech 116:103207. https://doi.org/10.1016/j.compgeo.2019.103207
13. Bendezu M, Romanel C, Roehl D (2017) Finite element analysis of blast-induced fracture propagation in hard rocks. Comput Struct 182:1–13. https://doi.org/10.1016/j.compstruc.2016.11.006
14. Wang ZL, Li YC, Shen RF (2007) Numerical simulation of tensile damage and blast crater in brittle rock due to underground explosion. Int J Rock Mech Min Sci 44:730–738. https://doi.org/10.1016/j.ijrmms.2006.11.004
15. Goodarzi M, Mohammadi S, Jafari A (2015) Numerical analysis of rock fracturing by gas pressure using the extended finite element method. Pet Sci 12:304–315. https://doi.org/10.1007/s12182-015-0017-x
16. Yazid A, Abdelkader N, Abdelmadjid H (2009) A state-of-the-art review of the X-FEM for computational fracture mechanics. Appl Math Model 33:4269–4282
17. Liu L, Li H, Li X, Wu R (2020) Full-field strain evolution and characteristic stress levels of rocks containing a single pre-existing flaw under uniaxial compression. Bull Eng Geol Environ 79:3145–3161
18. Liu L, Li H, Chen S et al (2021) Effects of bedding planes on mechanical characteristics and crack evolution of rocks containing a single pre-existing flaw. Eng Geol 293:106325
19. Donze FV, Bouchez J, Magnier SA (1997) Modeling fractures in rock blasting. Int J Rock Mech Min Sci 34:1153–1163
20. Bonilla-Sierra V, Scholtès L, Donzé F, Elmouttie M (2015) DEM analysis of rock bridges and the contribution to rock slope stability in the case of translational sliding failures. Int J Rock Mech Min Sci 80:67–78
21. Boon CW, Houlsby GT, Utili S (2015) Designing tunnel support in jointed rock masses via the DEM. Rock Mech Rock Eng 48:603–632
22. Li XF, Li HB, Liu YQ et al (2016) Numerical simulation of rock fragmentation mechanisms subject to wedge penetration for TBMs. Tunn Undergr Sp Technol 53:96–108
23. Li XF, Li X, Li HB et al (2018) Dynamic tensile behaviours of heterogeneous rocks: the grain scale fracturing characteristics on strength and fragmentation. Int J Impact Eng 118:98–118
24. Li XF, Zhang QB, Li HB, Zhao J (2018) Grain-based discrete element method (GB-DEM) modelling of multi-scale fracturing in rocks under dynamic loading. Rock Mech Rock Eng 51:3785–3817
25. Ning Y, Yang J, Ma G, Chen P (2011) Modelling rock blasting considering explosion gas penetration using discontinuous deformation analysis. Rock Mech Rock Eng. https://doi.org/10.1007/s00603-010-0132-3
26. Lisjak A, Grasselli G (2014) A review of discrete modeling techniques for fracturing processes in discontinuous rock masses. J Rock Mech Geotech Eng 6:301–314
27. Munjiza AA (2004) The combined finite-discrete element method. John Wiley & Sons
28. Munjiza A, Owen DRJ, Bicanic N (1995) A combined finite-discrete element method in transient dynamics of fracturing solids. Eng Comput. https://doi.org/10.1108/02644409510799532
29. Wu D, Li H, Shao Z et al (2021) Effects of infilling materials on mechanical behaviors and cracking process of pre-cracked rock: insights from a hybrid continuum-discontinuum method. Eng Fract Mech 253:107843
30. Wu D, Li H, Fukuda D, Liu H (2023) Development of a finite-discrete element method with finite-strain elasto-plasticity and cohesive zone models for simulating the dynamic fracture of rocks. Comput Geotech 156:105271
31. Fukuda D, Mohammadnejad M, Liu H et al (2019) Development of a GPGPU-parallelized hybrid finite-discrete element method for modeling rock fracture. Int J Numer Anal methods Geomech 43:1797–1824
32. Fukuda D, Liu H, Zhang Q et al (2021) Modelling of dynamic rock fracture process using the finite-discrete element method with a novel and efficient contact activation scheme. Int J Rock Mech Min Sci 138:104645
33. Yan C, Tong Y (2020) Calibration of microscopic penalty parameters in the combined finite–discrete-element method. Int J Geomech 20:4020092
34. Yahaghi J, Liu H, Chan A, Fukuda D (2021) Experimental and numerical studies on failure behaviours of sandstones subject to freeze-thaw cycles. Transp Geotech 31:100655

35. Li XF, Li HB, Liu LW et al (2020) Investigating the crack initiation and propagation mechanism in brittle rocks using grain-based finite-discrete element method. Int J Rock Mech Min Sci 127:104219. https://doi.org/10.1016/j.ijrmms.2020.104219
36. Lisjak A, Garitte B, Grasselli G et al (2015) The excavation of a circular tunnel in a bedded argillaceous rock (Opalinus Clay): short-term rock mass response and FDEM numerical analysis. Tunn Undergr Sp Technol 45:227–248
37. Lisjak A, Grasselli G, Vietor T (2014) Continuum-discontinuum analysis of failure mechanisms around unsupported circular excavations in anisotropic clay shales. Int J Rock Mech Min Sci 65:96–115. https://doi.org/10.1016/j.ijrmms.2013.10.006
38. Liu Q, Deng P (2019) A numerical investigation of element size and loading/unloading rate for intact rock in laboratory-scale and field-scale based on the combined finite-discrete element method. Eng Fract Mech 211:442–462
39. Han H, Fukuda D, Liu H et al (2020) Combined finite-discrete element modelling of rock fracture and fragmentation induced by contour blasting during tunnelling with high horizontal in-situ stress. Int J Rock Mech Min Sci. https://doi.org/10.1016/j.ijrmms.2020.104214
40. Zhao Q, Lisjak A, Mahabadi O et al (2014) Numerical simulation of hydraulic fracturing and associated microseismicity using finite-discrete element method. J Rock Mech Geotech Eng 6:574–581
41. Lei Z, Rougier E, Munjiza A et al (2019) Simulation of discrete cracks driven by nearly incompressible fluid via 2D combined finite-discrete element method. Int J Numer Anal Methods Geomech 43:1724–1743
42. Yan C, Zheng H, Sun G, Ge X (2016) Combined finite-discrete element method for simulation of hydraulic fracturing. Rock Mech Rock Eng. https://doi.org/10.1007/s00603-015-0816-9
43. An HM, Liu HY, Han H et al (2017) Hybrid finite-discrete element modelling of dynamic fracture and resultant fragment casting and muck-piling by rock blast. Comput Geotech 81:322–345. https://doi.org/10.1016/j.compgeo.2016.09.007
44. Yang P, Lei Q, Xiang J et al (2020) Numerical simulation of blasting in confined fractured rocks using an immersed-body fluid-solid interaction model. Tunn Undergr Sp Technol 98:103352
45. Wang B, Li H, Xing H, Li X (2022) Modelling of gas-driven fracturing and fragmentation in liquid CO2 blasting using finite-discrete element method. Eng Anal Bound Elem 144:409–421
46. Munjiza A, Knight EE, Rougier E (2015) Large strain finite element method: a practical course. John Wiley & Sons
47. Zienkiewicz OC, Taylor RL, Zhu JZ (2005) The finite element method: its basis and fundamentals. Elsevier
48. Deng P, Liu Q, Huang X et al (2021) Acquisition of normal contact stiffness and its influence on rock crack propagation for the combined finite-discrete element method (FDEM). Eng Fract Mech. https://doi.org/10.1016/j.engfracmech.2020.107459
49. Mahabadi OK, Lisjak A, Munjiza A, Grasselli G (2012) Y-Geo: new combined finite-discrete element numerical code for geomechanical applications. Int J Geomech 12:676–688. https://doi.org/10.1061/(asce)gm.1943-5622.0000216
50. Munjiza A, Rougier E, Lei Z, Knight EE (2020) FSIS: a novel fluid–solid interaction solver for fracturing and fragmenting solids. Comput Part Mech 7:789–805
51. Munjiza A, Latham JP, Andrews KRF (2000) Detonation gas model for combined finite-discrete element simulation of fracture and fragmentation. Int J Numer Methods Eng 49:1495–1520
52. Zhang Z-X (2016) Rock fracture and blasting: theory and applications. Butterworth-Heinemann
53. Park B-K, Lee I-M, Kim S-G, et al (2004) Probabilistic estimation of fully coupled blasting pressure transmitted to rock mass II-Estimation of rise time
54. Vanbrabant F, Chacón EP, Quiñones LA (2002) P and S Mach waves generated by the detonation of a cylindrical explosive charge–experiments and simulations. Fragblast 6:21–35
55. Ainalis D, Kaufmann O, Tshibangu JP et al (2017) Modelling the source of blasting for the numerical simulation of blast-induced ground vibrations: a review. Rock Mech Rock Eng. https://doi.org/10.1007/s00603-016-1101-2
56. Cho SH, Kaneko K (2004) Influence of the applied pressure waveform on the dynamic fracture processes in rock. Int J Rock Mech Min Sci 41:771–784. https://doi.org/10.1016/j.ijrmms.2004.02.006
57. Ning Y, Yang J, An X, Ma G (2011) Modelling rock fracturing and blast-induced rock mass failure via advanced discretisation within the discontinuous deformation analysis framework. Comput Geotech 38:40–49. https://doi.org/10.1016/j.compgeo.2010.09.003
58. Zhang ZX, Chi LY, Qiao Y, Hou DF (2021) Fracture initiation, gas ejection, and strain waves measured on specimen surfaces in model rock blasting. Rock Mech Rock Eng. https://doi.org/10.1007/s00603-020-02300-2
59. Lysmer J, Kuhlemeyer RL (1969) Finite dynamic model for infinite media. J Eng Mech Div 95:859–877
60. Tatone BSA, Grasselli G (2015) A calibration procedure for two-dimensional laboratory-scale hybrid finite-discrete element simulations. Int J Rock Mech Min Sci. https://doi.org/10.1016/j.ijrmms.2015.01.011
61. Mahabadi OK, Grasselli G, Munjiza A (2009) Numerical modelling of a Brazilian Disc test of layered rocks using the combined finite-discrete element method. In: RockEng09: 3rd Canada-US rock mechanics symposium. pp 87–88
62. Euser B, Rougier E, Lei Z et al (2019) Simulation of fracture coalescence in granite via the combined finite–discrete element method. Rock Mech Rock Eng 52:3213–3227
63. Yuan W, Wang W, Su X et al (2018) Numerical study of the impact mechanism of decoupling charge on blasting-enhanced permeability in low-permeability sandstones. Int J Rock Mech Min Sci. https://doi.org/10.1016/j.ijrmms.2018.04.029
64. Wang J, Elsworth D, Cao Y, Liu S (2020) Reach and geometry of dynamic gas-driven fractures. Int J Rock Mech Min Sci. https://doi.org/10.1016/j.ijrmms.2020.104287
65. Bhandari S (1980) On the role of stress waves and quasi-static gas pressure in rock fragmentation by blasting. In: Gasdynamics of Explosions and Reactive Systems. Elsevier, pp 365–383
66. McHugh S (1983) Crack extension caused by internal gas pressure compared with extension caused by tensile stress. Int J Fract 21:163–176
67. Lei Z, Rougier E, Knight EE, et al (2015) FDEM simulation on a triaxial core-flood experiment of shale. In: ARMA US Rock Mechanics/Geomechanics Symposium. ARMA, p ARMA-2015
68. Knight EE, Rougier E, Lei Z et al (2020) HOSS: an implementation of the combined finite-discrete element method. Comput Part Mech 7:765–787